

Attoampere Nanoelectrochemistry

Simon Grall, Ivan Alić, Eleonora Pavoni, Mohamed Awadein, Teruo Fujii, Stefan Müllegger, Marco Farina, Nicolas Clément,* and Georg Gramse*

Electrochemical microscopy techniques have extended the understanding of surface chemistry to the micrometer and even sub-micrometer level. However, fundamental questions related to charge transport at the solid-electrolyte interface, such as catalytic reactions or operation of individual ion channels, require improved spatial resolutions down to the nanoscale. A prerequisite for single-molecule electrochemical sensitivity is the reliable detection of a few electrons per second, that is, currents in the atto-Ampere (10^{-18} A) range, 1000 times below today's electrochemical microscopes. This work reports local cyclic voltammetry (CV) measurements at the solid-liquid interface on ferrocene self-assembled monolayer (SAM) with sub-atto-Ampere sensitivity and simultaneous spatial resolution < 80 nm. Such sensitivity is obtained through measurements of the charging of the local faradaic interface capacitance at GHz frequencies. Nanometer-scale details of different molecular organizations with a 19% packing density difference are resolved, with an extremely small dispersion of the molecular electrical properties. This is predicted previously based on weak electrostatic interactions between neighboring redox molecules in a SAM configuration. These results open new perspectives for nano-electrochemistry like the study of quantum mechanical resonance in complex molecules and a wide range of applications from electrochemical catalysis to biophysics.

to batteries.^[6] Additionally, it allows us to increase our understanding of molecular interactions in liquid, which is currently based on theoretical models of ensemble measurements. Towards these goals, scanning electrochemical microscopy (SECM), including the use of nanopipettes,^[7–9] has been developed to sense electrochemical reactions locally, providing spatial resolution of typically μm to the sub- μm range,^[10–12] but also fast reactions on nanometric particles could be resolved when well isolated.^[13,14] SECM techniques are now well-established for probing electrochemical systems at the micro- and nanoscale levels.^[15,16] Scanning probes have exploited redox-cycling amplification to reduce the electrode dimensions while keeping a reasonable signal level.^[11,17,18] Electrochemical scanning tunneling microscopy (EC-STM) has been used to study electrochemistry indirectly from a molecular electronics perspective.^[19,20] To date, these techniques have enabled measurements down to the fA (10^{-15} Ampere) range,^[11,21–25] which is still not sensitive


1. Introduction

Local electrical and electrochemical measurements and imaging at the nanoscale are crucial for the future development of molecular sensors,^[1] materials engineering,^[2] electro-physiology,^[3,4] and various energy applications from artificial photosynthesis^[5]

enough to obtain electrochemical signals at the nanoscale, except in the specific case of redox cycling amplification when ferrocene (Fc) is confined between 2 neighboring electrodes at the nanoscale.^[23,25] For the versatile measurement of electrochemical currents at the nanoscale aA (10^{-18} Ampere) sensitivity is crucial.

Dr. S. Grall, I. Alić, Dr. G. Gramse
Institute of Biophysics
Johannes Kepler University
Linz 4020, Austria
E-mail: georg.gramse@jku.at
Dr. E. Pavoni, Prof. M. Farina
Department of Information Engineering
Marche Polytechnic University
Ancona 60131, Italy

Prof. T. Fujii, Dr. N. Clément
LIMMS/CNRS
Institute of Industrial Science
University of Tokyo
Tokyo 153–8505, Japan
E-mail: nclement@iis.u-tokyo.ac.jp
Prof. S. Müllegger
Institute of Semiconductor and Solid-State Physics
Johannes Kepler University
Linz 4040, Austria
M. Awadein, Dr. G. Gramse
Keysight Labs Austria
Keysight Technologies
Linz 4020, Austria

 The ORCID identification number(s) for the author(s) of this article can be found under <https://doi.org/10.1002/smll.202101253>.

© 2021 The Authors. Small published by Wiley-VCH GmbH. This is an open access article under the terms of the Creative Commons Attribution-NonCommercial License, which permits use, distribution and reproduction in any medium, provided the original work is properly cited and is not used for commercial purposes.

DOI: 10.1002/smll.202101253

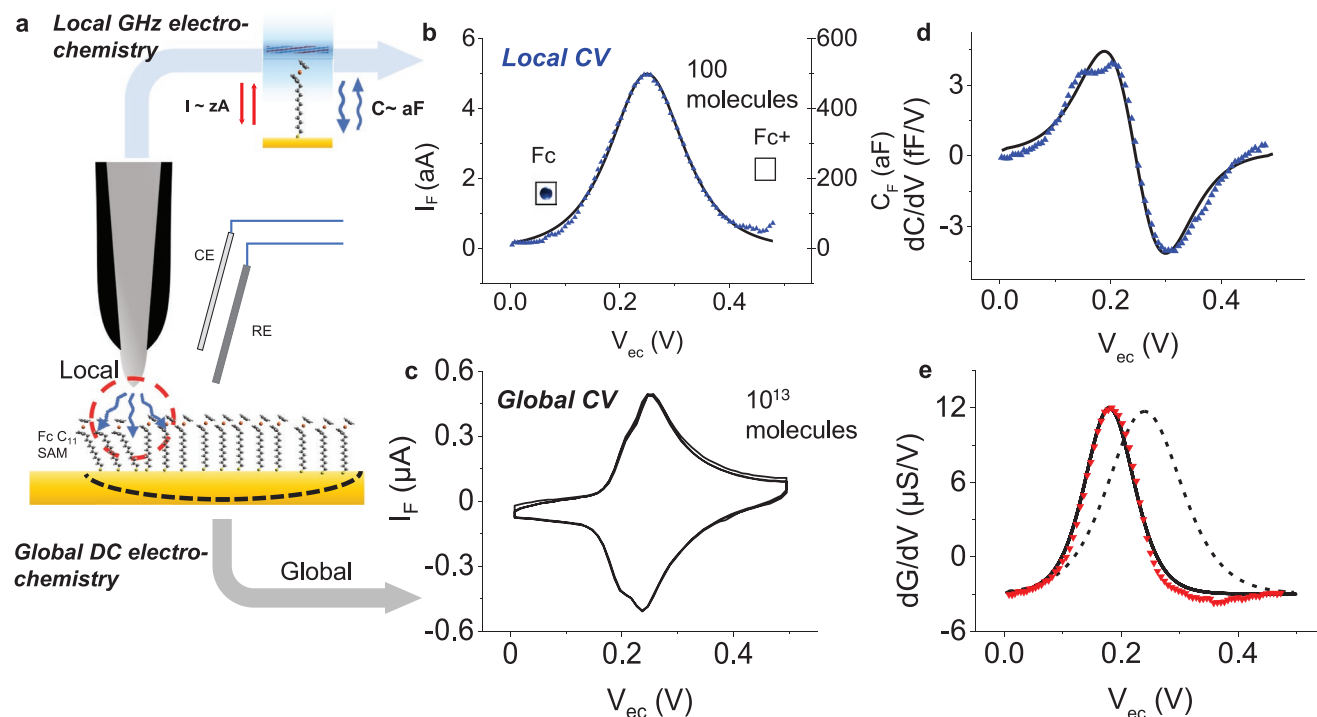


Figure 1. a) Schematic of the electrochemical RF-STC setup used in this work. b) Faradaic current I_F versus sample electrochemical potential, V_{ec} , recorded with the RF probe, a black line representing a Fermi distribution first derivative fit. c) DC cyclic voltammogram (CV) recorded at the same time by a potentiostat through the gold electrode. d) Capacitance derivative dC/dV CV, with the black line representing Fermi distributions second derivative. e) Conductance derivative dG/dV CV, with the solid and dashed lines representing Fermi distribution first-derivative fits. The solid line fitting the dG/dV datapoints and the dashed line show where the datapoints would be expected if centered on the same potential as in (b), (c), and (d). All data were recorded at a sweep rate $\nu = 10 \text{ mV s}^{-1}$.

Ferrocene^[26,27] is a well-known molecule in the literature and it is still among the many electrochemical systems reported to date whose electrochemical properties have remained unexplored at the nanoscale. Here, we report nanoscale cyclic voltammetry (CV) measurements with a sensitivity of about 120 Fc molecules bound to a gold surface. Our model system comprises a self-assembled monolayer (SAM) of Fc undecanethiol (Fc_{C11}) on Au(111). Similar systems have been recently reported for their promising applications, for example, as molecular memories, for high-frequency electronics through the THz gap, and as optical rectennas for solar cell applications without the Shockley–Queiser limitation.^[21,28]

We demonstrate how aA electrochemical measurements are achieved by sensing the faradaic capacitance variation associated with the electrochemical charge transfer. While a faradaic current I_F in the aA range cannot be measured directly due to an insufficient signal-to-noise ratio in pre-amplifiers, we show how it is possible to detect the associated aF capacitance C_F . We apply high-frequency techniques operating at a few GHz, where the admittance of the capacitance scales linearly with the frequency. The exceptionally high sensitivity of GHz admittance measurements combined with the advantages of nearfield detection in microwave microscopy has recently enabled breakthroughs in diverse areas of research, including semiconductor physics,^[29,30] molecular electronics,^[21] biophysics,^[31] and energy materials.^[32] To the best of our knowledge, the direct measurements of electrochemical charge transfer by microwave microscopy—reported herein—have not been reported previously.

2. GHz Readout of the Oxidation State at the Nanoscale by Cyclic Voltammetry

Figure 1 illustrates the powerful detection scheme of our radio frequency scanning tunneling microscope (RF-STC) heterodyne capacitive sensing method (scheme with technical details in Figure S1, Supporting Information). In particular, our method provides electrochemical information simultaneously on a global scale (black color) similar to conventional direct current (DC) CV measurement, and on a local scale, with an unprecedented spatial resolution (blue color). The global (macroscale) signal marked with a grey arrow in the bottom of Figure 1a is obtained under conventional DC conditions, yielding the respective macroscale CV curve shown in Figure 1c. It results from the electrochemical charge transfer reaction, which oxidizes and reduces the surface-bound Fc molecules, as it is well-known from the literature.^[33] Notice that the electrochemical current of the global signal is on the order of micro-Ampere. We have obtained the values of the half-wave potentials of $E_{1/2} = 0.241 \text{ V}$ and determined an average surface coverage of $\Gamma_T = 2.4 \pm 0.2 \text{ Fc molecules per nm}^2$ (Figure S2, Supporting Information), both values being in excellent agreement with literature.^[21] The double bump (shoulder) observed in the DC CV on Figure 1c is related to zones with larger roughness where electrostatic interactions between the Fc moieties are stronger.^[34]

In comparison, Figure 1b shows the local faradaic capacitance C_F and the corresponding local current signal I_F . Notice

that the faradaic current of the local signal is of the order of aA at the same sweep rate as in the global CV curve.

To understand this dramatic increase of sensitivity, consider that the faradaic current at the molecular level is based on the tunneling of electrons from the gold electrode to the Fc molecules, which accumulates charges (Q) at the Fc-liquid interface. In a simple picture, these charges attract ions in the solution and induce the formation of an electrical double layer with a capacitance C_{dl} . The faradaic current and the double layer are intrinsically coupled by the charge state of the Fc/Fc⁺ couple. The respective charge follows a Fermi distribution centered on the oxide-reduction potential V_0 of the Fc/Fc⁺ couple^[22,35] such that

$$Q(V_{ec}) = \Gamma_T q \left(1 + e^{-g \frac{(V_{ec} - V_0)F}{RT}} \right)^{-1} \quad (1)$$

where Γ_T is the surface coverage of Fc molecules, q the elementary charge, F is Faraday's constant, R is the gas constant, $g \approx 0.67$ a broadening factor, V_{ec} is electrochemical potential, and T is the temperature. Since capacitance is defined as $\Delta C = dQ/dV$, the change of capacitance in CV can be represented by first-order approximation as the derivative of the Fermi distribution (Equation (1)). Accordingly, dC/dV is expected to follow the second derivative of the Fermi distribution (Figure 1d,e, Note S1, Supporting Information). Finally, the electrochemical current at equilibrium I_F equals ΔC multiplied by the sweep rate $\nu = 10 \text{ mV s}^{-1}$ (Figure 1b).

Although the local capacitance is extremely small (aF level), it can be measured by up-conversion to GHz frequencies. For this, we have combined an EC-STM setup with a vector network analyzer (VNA) utilizing a high-frequency transmission line between the local probe and the VNA as shown in Figure 1a (detailed version in Figure S1, Supporting Information). Topography feedback is maintained by sensing the tunneling current between the tip and the conducting substrate. In addition, we have implemented bipotentiostatic control of both the substrate and probe, which enables stable STM feedback in the electrolyte for topographic imaging simultaneously with local CV. We used a PtIr probe coated with electrically insulating wax,^[36] exposing only the last 10–100 nm of the tip apex to the electrolyte (Figure S8, Supporting Information); our probe facilitates a background current of <10 pA (Figure S3, Supporting Information).

The VNA measures the $S_{11}(V_{ec})$ reflection coefficient of the microwave signal while keeping the Fc molecules at electrochemical potential V_{ec} . It is proportional to the capacitance and conductance changes below the tip and scales linearly with frequency ($S_{11} \propto \omega C_F$, Figure S1, Supporting Information). To resolve the extremely small faradaic capacitance variations of a few molecules on top of the background capacitance of the cables and the upper part of the STM probe, we have implemented a variable interferometric matching circuit that offsets the background impedance and solely amplifies the impedance variation sensed by the probe (Figure S1, Supporting Information). With this matching network, we typically achieve a sensitivity of $\Delta C \approx 2 \text{ aF}$ at 2 GHz, which corresponds to a conductance $\Delta G \approx 25 \text{ nS}$.^[37] We note that, increasing the detection frequency further would increase the sensitivity in the capacitance channel, but the well-known dielectric loss of water at these frequencies^[38,39] would annihilate this advan-

tage. Although direct $S_{11}(V_{ec})$ cycles lead to favorable signal-to-noise ratios, they are subjected to crosstalk with the topography measured by the STM current, and electrochemical activity becomes difficult to distinguish from topographic variations. In order to increase further the sensitivity and selectivity for the electron transfer of the surface-bound electrochemical species, we apply additional kHz modulation of the substrate potential V_{ec} . This signal modulates the electrochemical electron transfer, which is detected by a lock-in amplifier acquiring the complex derivative signal, dS_{11}/dV , corresponding to dC/dV and dG/dV . All contributions independent of V_{ec} are suppressed. The measured capacitance CV curve and the respective derivative dC/dV displayed in Figure 1b and Figure 1d are very similar to those of an ideal redox SAM at equilibrium as described by Equation (1). We estimate by fitting that the capacitance peak in the CVs would correspond to the charge transfer of Fc molecules in an area with a diameter of approximately $96 \pm 32 \text{ nm}$ (Note S2, Supporting Information) and a signal sensitivity of 120 molecules at 2 aF noise floor. We remark that for semi-quantitative analysis, the CVs obtained at the nanoscale by our RF-STM setup can be directly compared to ensemble measurements, providing an extremely versatile method to acquire nanoelectrochemical images. Small deviations from this simple model will be discussed further below like, for example, the double bump only visible in the dC/dV curve (Figure 1d) and the presence of the dG/dV signal itself (Figure 1e).

3. Nanoscale Molecular Organization

Our RF-STM method allows for topography imaging and independent detection of the molecules' electrochemical oxidation state on the electrode surface. Figure 2a shows the 3D topography and local capacitance (color scheme) of a FcC₁₁ SAM on gold at an electrochemical potential of $V_{ec} = 150 \text{ mV}$, close to its electrochemical redox potential. Moreover, the 3D color maps show the capacitance recorded between $V_{ec} = 50$ and 200 mV over the same image frame by sweeping V_{ec} at 5 mV s^{-1} during the acquisition. For better clarity, Figure 2c shows the histogram of consecutively recorded capacitance maps, exhibiting two peaks corresponding to the bright and dark areas in the maps. The peaks are separated by $C_{12} = 20 \text{ aF}$. Although it is known that thiol monolayers may form different molecular organizations,^[40] our RF-STM results (Figure 2) demonstrate the successful discrimination of subtle differences in electrochemical activity with unprecedented sensitivity and spatial resolution. Interestingly, a density difference of only $19 \pm 1\%$ (Figure S4, Supporting Information) between the two molecular organizations was obtained, a feature that ensemble measurements cannot resolve. This finding is also in agreement with the theoretical prediction that electrostatic interactions between Fc molecules of the same molecular organization phase should negligibly affect the CV shape.^[22] To our knowledge, no other technique allows the resolution of such a small difference at the nanoscale. With further optimization of the STM stability and electrical detection circuitry, we will, in the future, also achieve molecular resolution such as the one displayed by Rudnev et al.^[41]

As shown in Figure 2b, no crosstalk between signals was observed. The lateral resolution of the microwave channels

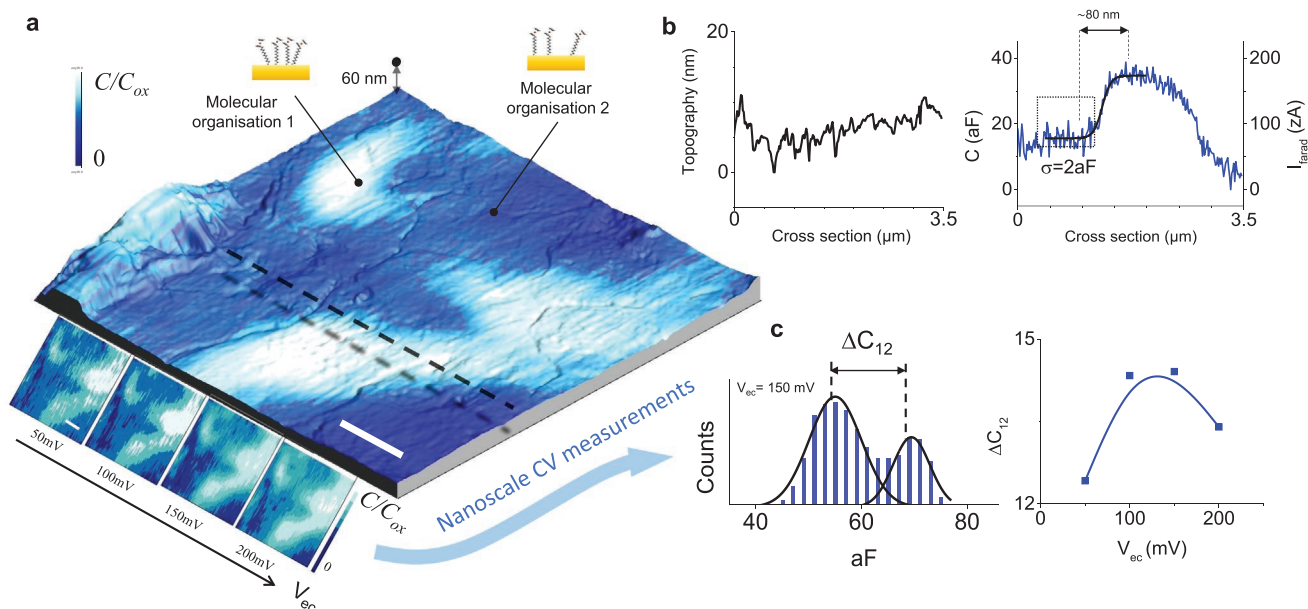


Figure 2. a) 3D representation of a SAM of FcC₁₁ grafted on gold at an electrochemical potential (V_{ec}) of 150 mV. The voltage was swept at $v = 5 \text{ mV s}^{-1}$ on the sample during this experiment. The color overlay represents the capacitance C (at $V_{ec} = 150$ mV), and the color maps below the 3D image represent the capacitance on the same sample between 0 mV and 200 mV. Scale bar is 800 nm. b) Cross-section corresponding to the dashed line in (a) showing the topography and the capacitance channels. No crosstalk is observed, and a lateral resolution of approximately 80 nm is obtained for the capacitance channel. The capacitance is converted into current knowing the sweep rate ($v = 5 \text{ mV s}^{-1}$), which gives a current on the order of 150 zA. c) Histograms of C color maps at $V_{ec} = 50$ mV. The two peaks are distinguishable and correspond to the two areas visible on the capacitance overlay in (a). The peak distance (ΔC_{12}) is plotted versus the electrochemical potential V_{ec} . The solid line on the ΔC_{12} plot is a guide to the eye.

is determined to approximately 80 nm from the line profile. This agrees well with the sensitivity of 96 nm estimated from the FcC₁₁ SAM density and the data of Figure 1d (Notes S2 and S3, Supporting Information). The measured data were scaled with a capacitance noise value of 2 aF, as detailed in the methods section. To increase the accuracy, metrological calibration based on calibration kits or retract curves^[42] can be implemented in the future.

4. High Frequency Dynamics of Electron Transfer

In the equivalent circuit model in Figure 3a, we visualize the coupling of faradaic pseudo-capacitance $C_F(V_{ec})$ and the double layer capacitance $C_{dl}(Q(V_{ec}))$ at the frequencies applied in our experiments. Note that also the geometric capacitance C_{SAM} (voltage-independent) and bulk water capacitance C_w (tip-to-sample distance-dependent) are included. While this model shows only capacitive components, we have to consider also the conductivity of the ionic media and out-of-equilibrium effects in the other components. Finite element models (FEMs) (Figure 3a) can account for the deviations from the simple Fermi-level approximation. Most importantly, at GHz frequencies well above the electron transfer rate constant k_{ET} , the charges responsible for C_F are too slow to follow the electric field,^[32] and only the double layer capacitance induced by the charges at the solid-liquid interface $C_{dl} = dQ/dV$ is measured (Note S3, Supporting Information). Resistive out-of-equilibrium effects are also the origin of the dG/dV signal (Figure 1e). An important feature is that the RF conductance is very large compared to the DC tunnel conductance and does not show the characteristic exponential probe-sample distance dependency of

a tunneling process, but it changes as the $dC/dV(d)$ curves only moderately with distance d (Figure S5, Supporting Information). At a close distance ($d < 200$ nm), the $dC/dV(V_{ec})$ curve for oxidation of the surface-bound Fc was measured (Figure 3b). Meanwhile, only at $d > 200$ nm above the surface, the signal became insensitive to the electrochemical species.

Our FEM numerical simulations of the tip-sample system that capture these experimental observations are based on the Nernst–Planck–Poisson equations (as detailed in the methods section), and the potential distribution at the tip sample region both in the DC and GHz frequency regimes is shown together with an effective equivalent circuit model in Figure 3a. Only the very end of the probe was exposed to the solution, while the upper part of the probe was isolated by a dielectric material. The DC potential completely dropped off in isolation, as expected; while at 1 GHz, the dielectric isolation was less effective but still led to a considerable potential drop and focusing effect, making the measurement more local. At the exposed part of the probe, only in the GHz regime, where the ions can hardly follow the field, the double-layer capacitance starts to relax. This agrees with the experimentally obtained dC/dV curve shown in Figure 3b, obtained well above the surface, which follows the hyperbolic dependency of the diffusive layer capacitance with respect to the applied electrochemical potential. However, at a close tip-sample distance, the relaxation time diminished again^[43] (Note S3, Supporting Information).

Simulation of the spectra at a close distance (2 nm) above the SAM showed the experimentally observed peak in the conductance channel (compare Figure 3c and 1e), which is related to the increased number of ions compensating the Fc/Fc⁺ charge at the interface. Even the shoulder in the dC/dV signal

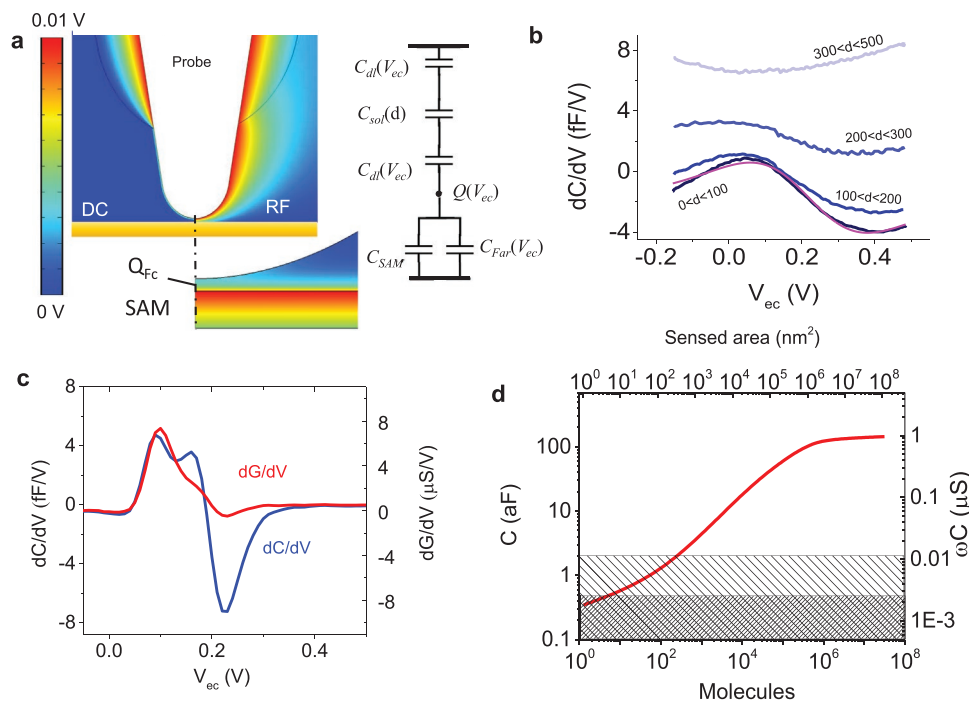


Figure 3. a) Finite element modeling (FEM) and equivalent circuit of the insulated tip over the SAM, showing the direct current and radiofrequency regimes for the FEM. The zoom-in below shows the potential distribution in the SAM. b) Experimental dC/dV acquired at different distances during a potential sweep ($v = 5 \text{ mV s}^{-1}$) on the gold with grafted FcC_{11} SAM. c) Simulated dG/dV and dC/dV curves with the probe at $d = 2 \text{ nm}$ and the experimental conditions as in Figure 1b. d) Sensitivity analysis of the capacitance signal. The expected capacitance signal as a function of the covered FcC_{11} area, and the number of molecules is calculated. Light and densely dashed areas correspond to the sensitivity limit of the measurements in Figure 1 and optimized sensitivity conditions at a lower bandwidth of 100 Hz, respectively.

is recovered (Figure 1d), which could not be retrieved with the simple Fermi distribution. Therefore, the presence of ions in the solution and the diffusive double layer must be considered to obtain a quantitative agreement between the measured and calculated capacitance and conductance signals. From our FEM results, we calculated the expected capacitance contrast between the substrate and an electrochemical active Fc layer of varying size (Figure 3d). Assuming the typical electrical sensitivity of 2 aF we obtained under the here reported measurement conditions, the simulations suggest that the charge transfer of as few as 200 Fc molecules could be still experimentally resolved, which is in good agreement with the approximation from the above section. Moreover, we estimate that the detection sensitivity could be still improved to about 0.5 aF (i.e., by better matching and at the cost of detection bandwidth) such that even tens of Fc molecules could be resolved.

Of note, the charge transfer to Fc is a function of time, reaction rate, and voltage; thus, it is a dynamic process. Although the GHz modulation is faster than the reaction rate, appropriate selection of the kHz modulation frequency would allow for the extraction of the dynamic properties of the molecular charge transfer, while the appropriate selection of the RF frequency and scan distance would allow the double layer dynamics to be investigated (Note S3, Supporting Information). Both topics will be further addressed in future research. The present study was performed on flat and conductive surfaces, since the STM approach is limited to such surfaces.^[11] Nevertheless, the RF faradaic current sensing could also be implemented in combination with an atomic force microscope

(AFM), or a shear force SECM which would allow imaging of a wider range of materials including nanoarray, etc.

5. Conclusion

In conclusion, we have shown how electrochemical microwave microscopy locally resolves redox reactions of as few as 120 molecules, which corresponds to the transfer of the same number of elementary charges. To reach the required aA current sensitivity, we detected the oxidation and reduction of the surface-bound redox species at microwave frequencies and amplified our sensitivity dramatically while maintaining the bandwidth. At these frequency ranges that are well above the electrochemical rate constants, we sense the change of the faradaic capacitance instead of the current. We show by finite element simulations that this high-frequency capacitive coupling to electrochemical reactions is only possible at the nanoscale. Our technique sets the groundwork for a wide range of applications, including molecular memories, electrochemical catalysis, charge transport in molecular biophysics, and the study of quantum mechanical resonance effects in complex molecules, which were completely inaccessible until now.

6. Experimental Section

Electrochemical Setup: The experimental setup is described in Figure 1 and Figure S1, Supporting Information. It consisted of an RF-STM

microscope and a potentiostat connected to a Pt counter electrode (CE), an Ag/AgCl reference electrode (RE), a gold (111)-on-mica substrate as working electrode (Figure S7, Supporting Information) (Phasis, Switzerland) (WE), and the RF-STM microscope tip as second working electrode (PtIr, 80/20). A SAM of Fc undecanethiol (FcC₁₁) was grafted on the gold substrates by incubation in 1 mM FcC₁₁ (Sigma Aldrich) in ethanol for at least 12 h in closed vials in ambient conditions. The gold-on-mica samples were only blue-flamed before the incubation, and rinsed with ethanol after incubation. Since an STM-based measurement setup is used, it is not desirable to have a densely packed monolayer that may hinder the tunneling with reported thicknesses of 1.8 nm for such FcC₁₁ SAMs.^[44] The samples were placed in a homemade electrochemical cell. Bottom contact for bias and electrochemical potential sweeping was made using silver paste. The electrochemistry was done in 10 mM NaClO₄ water solution bubbled with nitrogen immediately before every experiment. All parts of the setup were controlled through the microscope's controller and software (Keysight).

RF Setup: The RF-STM consisted of a 5400 Keysight AFM mount and an STM scanner modified for RF modulation at the tip. A bias tee separated low-frequency currents (tunneling and DC faradaic currents) and the RF signal. A VNA (Keysight) served as the RF source. The RF transmission line is described in Figure S1, Supporting Information, and consisted of an interferometric setup comprising a voltage-controlled attenuator, a directional coupler, and a hybrid coupler. An AC voltage of 50 mV was applied to the sample with a frequency ranging from 30 to 80 kHz depending on the experiment. The reflected signal (S₁₁) was obtained from the VNA and the derivative of S₁₁ versus the AC voltage applied to the sample (dS₁₁/dV) was obtained after direct down-modulation of the outgoing RF signal in a mixer. Therefore, the outgoing RF signal was multiplied with the back-reflected signal, which has been amplified by a low noise amplifier. This down modulated signal was fed into a lock-in amplifier giving the amplitude and phase of dS₁₁/dV. By introducing this additional low frequency (kHz) electrical modulation between the substrate and the probe, the drift was removed and dramatically improved the sensitivity to the electrochemical reaction (see also Note S4, Supporting Information). Stable measurements with high RF resolution were possible for over half a day. The main limitation for this duration was the evaporation in the electrochemical cell, which was not optimized for extended measurements.

Data Scaling: In order to map complex S₁₁ data to the complex admittance plane Y, containing a conductance channel (ΔG) and a capacitance channel (ΔC), small variations were assumed in S₁₁ and used the first-order approximation relationship:

$$\Delta S_{11} = ae^{i\phi} \Delta Y = ae^{i\phi} (\Delta G + i\omega \Delta C) \quad (2)$$

While *a* defines the scaling of the admittance with respect to the measured S₁₁ signal, *φ* defines the rotation in the complex plane. The scaling factor *a* can be obtained by assessing the noise obtained on S₁₁ data, and comparing it with the noise floor obtained on independent measurements in a dry environment. In the measurement frequency, the noise floor was found to be around 2 aF for capacitances measured using such techniques.^[42,45] Being aware that the data presented here were obtained from the integration of dS₁₁/dV, a similar estimation of *G* from S₁₁ data was done and led to results similar to the *G* obtained out of dS₁₁/dV (Figure S6 and Note S5, Supporting Information). Though S₁₁ signals suffered from significantly more crosstalk with topography and barely exhibited a capacitance signal (which was expected here because of stray capacitances), this confirmed that the estimation of the capacitance and conductance from the noise on the integrated values of dS₁₁/dV was not arbitrary.

Finite Element Modeling: FEM was carried out with COMSOL Multiphysics 5.5 (2D axisymmetric, Nernst-Planck-Poisson Equations, statics, time domain, frequency domain perturbation). The simulation geometry for quantification resembles the experimental conditions and is shown in Figure 3a. The model consisted of a 5 μm high STM probe modeled as a truncated cone with a cone angle of 15°. The tip has a spherical apex with a radius of 100 nm and was located at a

distance *d* above the sample. The SAM was modeled as a 1.5 nm thick dielectric layer with a dielectric permittivity of 2. The voltage-dependent surface charge on the SAM was calculated according to Equation (1) using the Boundary ODE interfaces. To achieve accurate results and convergence of the solution, meshing was set to 0.1 nm on the exposed probe surface and the SAM using the boundary layer mesh. For the time-dependent solution probe and substrate were set to apply the voltage sweep identical to the experiment and the upper part of the simulation box was set to ground. Concentration on the upper part of the simulation box was set to 10 mM. For the frequency perturbation step, the Terminal was set to the probe and the ground was set to the substrate. With this model, the C(V) and G(V) voltage sweeps were calculated and differentiated.

Supporting Information

Supporting Information is available from the Wiley Online Library or from the author.

Acknowledgements

This project has received funding from the ATTRACT project funded by the European Commission under Grant Agreement 777222. Additional support from the European Research Council under the European Union's Horizon 2020 (EU's H2020) research and innovation programme under Grant Agreement 771193, the NanoBat project funded from EU's H2020 research and innovation programme under Grant Agreement no. 861962, the MSCA-ITN project BORGES under grant agreement 813863 and the Austrian FWF Project P28018-B27 is acknowledged. The authors would also like to thank Dominik Farika and Nicolas Lesniewska, who helped greatly on the preliminary experimental setup, David Toth, for the invaluable inputs and discussions during experimental processes and Peter Pohl for his support.

Conflict of Interest

The authors declare no conflict of interest.

Data Availability Statement

The data that support the findings of this study are available from the corresponding author upon reasonable request.

Keywords

attoampere, nano-electrochemistry, radiofrequency, scanning tunneling microscopy

Received: March 2, 2021

Revised: April 19, 2021

Published online: June 13, 2021

- [1] R. Sivakumarasamy, R. Hartkamp, B. Siboulet, J.-F. Duf r che, K. Nishiguchi, A. Fujiwara, N. Cl ment, *Nat. Mater.* **2018**, *17*, 464.
- [2] M. Stefanoni, U. M. Angst, B. Elsener, *Nat. Mater.* **2019**, *18*, 942.
- [3] J. Abbott, T. Ye, L. Qin, M. Jorgolli, R. S. Gertner, D. Ham, H. Park, *Nat. Nanotechnol.* **2017**, *12*, 460.
- [4] D. L. Gonzales, K. N. Badhiwala, D. G. Vercosa, B. W. Avants, Z. Liu, W. Zhong, J. T. Robinson, *Nat. Nanotechnol.* **2017**, *12*, 684.

- [5] K. K. Sakimoto, A. B. Wong, P. Yang, *Science* **2016**, 351, 74.
- [6] F. Liu, G. Sun, H. B. Wu, G. Chen, D. Xu, R. Mo, L. Shen, X. Li, S. Ma, R. Tao, X. Li, X. Tan, B. Xu, G. Wang, B. S. Dunn, P. Sautet, Y. Lu, *Nat. Commun.* **2020**, 11, 5215.
- [7] K. Jayant, J. J. Hirtz, I. J. -L. Plante, D. M. Tsai, W. D. A. M. De Boer, A. Semonche, D. S. Peterka, J. S. Owen, O. Sahin, K. L. Shepard, R. Yuste, *Nat. Nanotechnol.* **2017**, 12, 335.
- [8] Y. Takahashi, A. Kumatani, H. Munakata, H. Inomata, K. Ito, K. Ino, H. Shiku, P. R. Unwin, Y. E. Korchev, K. Kanamura, T. Matsue, *Nat. Commun.* **2014**, 5, 5450.
- [9] B. Ballesteros Katemann, A. Schulte, W. Schuhmann, *Chem. - Eur. J.* **2003**, 9, 2025.
- [10] X. Shi, W. Qing, T. Marhaba, W. Zhang, *Electrochim. Acta* **2020**, 332, 135472.
- [11] K. Chennit, J. Trasobares, A. Anne, E. Cambriil, A. Chovin, N. Clément, C. Demaille, *Anal. Chem.* **2017**, 89, 11061.
- [12] Y. Liang, J. H. K. Pfisterer, D. McLaughlin, C. Csoklich, L. Seidl, A. S. Bandarenka, O. Schneider, *Small Methods* **2019**, 3, 1800387.
- [13] T. Sun, Y. Yu, B. J. Zacher, M. V. Mirkin, *Angew. Chem.* **2014**, 126, 14344.
- [14] M. V. Mirkin, T. Sun, Y. Yu, M. Zhou, *Acc. Chem. Res.* **2016**, 49, 2328.
- [15] C. G. Zoski, *J. Electrochem. Soc.* **2016**, 163, H3088.
- [16] A. J. Bard, M. V. Mirkin, *Scanning Electrochemical Microscopy*, 2nd ed., CRC Press, Boca Raton, USA **2012**.
- [17] A. J. Bard, F.-R. F. Fan, *Acc. Chem. Res.* **1996**, 29, 572.
- [18] A. Anne, E. Cambriil, A. Chovin, C. Demaille, *Anal. Chem.* **2010**, 82, 6353.
- [19] C. Huang, A. V. Rudnev, W. Hong, T. Wandlowski, *Chem. Soc. Rev.* **2015**, 44, 889.
- [20] M. López-Martínez, J. M. Artés, V. Sarasso, M. Carminati, I. Díez-Pérez, F. Sanz, P. Gorostiza, *Small* **2017**, 13, 1700958.
- [21] J. Trasobares, D. Vuillaume, D. Théron, N. Clément, *Nat. Commun.* **2016**, 7, 12850.
- [22] J. Trasobares, J. Rech, T. Jonckheere, T. Martin, O. Alevéque, E. Levillain, V. Díez-Cabanes, Y. Olivier, J. Cornil, J. P. Nys, R. Sivakumarasamy, K. Smaali, P. Leclere, A. Fujiwara, D. Théron, D. Vuillaume, N. Clément, *Nano Lett.* **2017**, 17, 3215.
- [23] *Applications of Electrochemistry and Nanotechnology in Biology and Medicine II* (Ed: N. Eliaz), Springer US, Boston, MA **2012**.
- [24] D. J. Müller, Y. F. DuFrène, *Nat. Nanotechnol.* **2008**, 3, 261.
- [25] S. G. Lemay, S. Kang, K. Mathwig, P. S. Singh, *Acc. Chem. Res.* **2013**, 46, 369.
- [26] R. R. Gagne, C. A. Koval, G. C. Lisensky, *Inorg. Chem.* **1980**, 19, 2854.
- [27] A. M. Bond, E. A. McLennan, R. S. Stojanovic, F. G. Thomas, *Anal. Chem.* **1987**, 59, 2853.
- [28] C. A. Reynaud, D. Duché, J.-J. Simon, E. Sanchez-Adaimé, O. Margeat, J. Ackermann, V. Jangid, C. Lebouin, D. Brunel, F. Dumur, D. Gigmes, G. Berginc, C. A. Nijhuis, L. Escoubas, *Prog. Quantum Electron.* **2020**, 72, 100265.
- [29] G. Gramse, A. Kölker, T. Škerek, T. J. Z. Stock, G. Aeppli, F. Kienberger, A. Fuhrer, N. J. Curson, *Nat. Electron.* **2020**, 3, 531.
- [30] P. Ponath, K. Fredrickson, A. B. Posadas, Y. Ren, X. Wu, R. K. Vasudevan, M. Baris Okatan, S. Jesse, T. Aoki, M. R. McCartney, D. J. Smith, S. V. Kalinin, K. Lai, A. A. Demkov, *Nat. Commun.* **2015**, 6, 6067.
- [31] M. C. Biagi, R. Fabregas, G. Gramse, M. Van Der Hofstadt, A. Juárez, F. Kienberger, L. Fumagalli, G. Gomila, *ACS Nano* **2016**, 10, 280.
- [32] A. Tselev, J. Velmurugan, A. V. Ilevlev, S. V. Kalinin, A. Kolmakov, *ACS Nano* **2016**, 10, 3562.
- [33] A. L. Eckermann, D. J. Feld, J. A. Shaw, T. J. Meade, *Coord. Chem. Rev.* **2010**, 254, 1769.
- [34] N. Nerngchamnong, D. Thompson, L. Cao, L. Yuan, L. Jiang, M. Roemer, C. A. Nijhuis, *J. Phys. Chem. C* **2015**, 119, 21978.
- [35] E. Laviron, *J. Electroanal. Chem. Interfacial Electrochem.* **1979**, 100, 263.
- [36] L. A. Nagahara, T. Thundat, S. M. Lindsay, *Rev. Sci. Instrum.* **1989**, 60, 3128.
- [37] S.-S. Tuca, M. Kasper, F. Kienberger, G. Gramse, *IEEE Trans. Nanotechnol.* **2017**, 16, 991.
- [38] U. Kaatz, *J. Chem. Eng. Data* **1989**, 34, 371.
- [39] R. Buchner, J. Barthel, J. Stauber, *Chem. Phys. Lett.* **1999**, 306, 57.
- [40] K. Smaali, *ACS Nano* **2012**, 6, 9.
- [41] A. V. Rudnev, K. Yoshida, T. Wandlowski, *Electrochim. Acta* **2013**, 87, 770.
- [42] G. Gramse, M. Kasper, L. Fumagalli, G. Gomila, P. Hinterdorfer, F. Kienberger, *Nanotechnology* **2014**, 25, 145703.
- [43] M. Z. Bazant, K. Thornton, A. Ajdari, *Phys. Rev. E* **2004**, 70, 021506.
- [44] S. Watcharinyanon, E. Moons, L. S. O. Johansson, *J. Phys. Chem. C* **2009**, 113, 1972.
- [45] F. Wang, N. Clément, D. Ducatteau, D. Troadec, H. Tanbakuchi, B. Legrand, G. Dambrine, D. Théron, *Nanotechnology* **2014**, 25, 405703.